INDIAN JOURNAL OF SCIENCE AND TECHNOLOGY

RESEARCH ARTICLE

Corrosion and Tribological Studies on Additively Manufactured Gyroid Ti-6Al-4V with Varied Porosity Percentage for Orthopaedic Application

L Daniel Devaraj[1]*, V Srinivasan[2], S Selvabharathi[3]

1 Reseach Scholar, Department of Manufacturing Engineering, Faculty of Engineering and Technology, Annamalai University, Annamalai Nagar, 608 002, Tamil Nadu, India
2 Associate Professor, Department of Manufacturing Engineering, Faculty of Engineering and Technology, Annamalai University, Annamalai Nagar, 608 002, Tamil Nadu, India
3 M. E Student, Department of Manufacturing Engineering, Faculty of Engineering and Technology, Annamalai University, Annamalai Nagar, 608 002, Tamil Nadu, India

OPEN ACCESS

Received: 27-07-2023
Accepted: 11-09-2023
Published: 25-10-2023

Citation: Devaraj LD, Srinivasan V, Selvabharathi S (2023) Corrosion and Tribological Studies on Additively Manufactured Gyroid Ti-6Al-4V with Varied Porosity Percentage for Orthopaedic Application. Indian Journal of Science and Technology 16(40): 3443-3452. https://doi.org/10.17485/IJST/v16i40.1882

* **Corresponding author**.

danieldevament96@gmail.com

Funding: None

Competing Interests: None

Published By Indian Society for Education and Environment (iSee)

ISSN
Print: 0974-6846
Electronic: 0974-5645

Abstract

Objectives: To evaluate the tribological and corrosive characteristics of an additively printed gyroid Ti-6Al-4V for Bio medical implant application. **Methods**: Direct Metal Laser Sintering with regulated input process parameters were used to print the samples. Corrosion investigations have been completely investigated using Potentiodynamic polarization under simulated body fluid conditions. The wear parameters for the samples were maintained with normal load ranging from 10 to 50 N, with sliding velocity ranging from 0.5 to 1.5 m/s for a sliding distance of 1000 m. The further study investigates the impact of load and velocity on the coefficient of friction (COF) and wear rate of the Gyroid samples. **Findings**: According to the results obtained, the material with the highest resistance to corrosion is exhibited by gyroid lattice Ti-6Al-4V that has a porosity of 60%. These samples exhibited by a worn-out rate of 2 x 10-11 m^3/m and 5.3 x 10-11 m^3/m for the normal load of 10 N and 50 N respectively. Minimum wear rate of 3.3 x 10-11 m^3/m was obtained for a sliding velocity of 0.5 m/s, where a maximum wear rate was obtained at 1.5 m/s of 3.7 x 10-11 m^3/m. Sample C has better tribological properties and is shown good wear resistance, when compared to sample A & B, which is attributed to the highest micro hardness of sample C of 467 HV. **Novelty:** The work presented in this study exhibits a unique approach by fabricating a gyroid lattice structure with varying levels of porosity. The limited availability of literature on tribological and corrosion issues necessitates the identification of a unique research need. An investigation of the effect of wear mechanisms on the tribological features of Gyroid Ti-6Al-4V is considered to be a unique research attempt.

Keywords: Ti6Al4V; Direct Metal Laser Sintering technology; Microhardness; Potentiodynamic Polarization; Tribology; Biomedical implants

1 Introduction

Metal implant during surgery is a structural element used to reinforce the bone and its joints. A set of implants comprises compression plates fastened to the bone using bolts and nuts. This is especially helpful when conventional techniques (apart from implants) could result in cartilage atrophy and body joints that are just lengthy[(1)]. The chemical constitution of Ti alloys used for biomedical purposes has been investigated because of the corrosive condition which enables the escape of implant ions to nearby tissues or organs that are distant by body fluids, which has a significant impact on the success of the recovery and long-term wellness.[(2)]

Despite having advantageous properties such as resistance to corrosion, mechanical characteristics, biological properties to the biological situation, reduced young's modulus, less weight, high strength and outstanding clinical responses, they have a tendency to release toxic ions that cause immune and inflammatory reactions that result in implant loss. Furthermore, they lack inherent antibacterial properties and are not bioactive[(3)]. Due to its superior mechanical qualities and resistance to corrosion, Ti-6Al-4V has been employed in medical applications. However, it contains chemical components that, if released into bodily fluids, might cause allergies and even cancer[(4)].

Corrosion potential is affected by the passive oxide layer formation, temperature, rate of corrosion, and an electrolyte. As a result, an interaction between the biological environment and the morphological, mechanical, and physiochemical properties of an oxide of titanium that forms suddenly on the implant surface and provides resistance to corrosion is directly related to titanium alloy biocompatibility[(5)].

Based on the studies the increased proportions of formation of new bone in the sample with porous structures, indicate that the development of void space is a leading optimization method for bone integration and enhancing load sharing capabilities of an implant. The gyroid is a typical TPMS structure used in lattice-based implants. This is frequently chosen because it has the ideal characteristics of a substantial surface-to-volume ratio, a smooth transition between unit cells, excellent durability, and the capacity to endure severe loads[(6)].

According to Li et al.'s study of the 60% porosity and 80% porosity of gyroid test samples were taken, the 60% samples had enhanced osseointegration rates and mechanical attachment a biocritical defect model's robustness, whereas the 80% porosity samples showed declining bone in growth and strength. The findings demonstrate that the alloy's wear mechanism transforms between 0.4 and 1.0 m/s of scratch speed and that as scratch increases in speed, the wear rate reduces[(7)].

Sl.no	Title	Author	Remarks
1.	Surface curvature in triply-periodic minimal surface architectures as a distinct design parameter in preparing advanced tissue engineering scaffolds	S.B. Blanquer, et al.	In-depth studies on the impact of TPMS scaffold surface curvature on porosity, permeability, and surface morphology were carried out by Blanquer et al[(8)].
2.	Study on corrosion resistance and biotribological behavior of porous structure based on the SLM manufactured medical Ti6Al4V	Lu, P, et al.	corrosion resistance of Ti6Al4V components produced using selective laser melting (SLM) was significantly enhanced. Specifically, at a laser power of 200 W, the corrosion voltage was measured to be -0.352 V[(9)].
3.	Influence of the synthesis technique on tribological behavior of a Ti-6Al-4V alloy.	Martinez, C et al.	The tribological characteristics of pure Ti and Ti6Al4V in Hanks solution were examined. Their findings confirmed the presence of fractures on the samples, accompanied with prevalent abrasive wear[(10)].
4.	Compressive behaviour of gyroid lattice structures for human cancellous bone implant applications.	Yánez, A et al.	In this study, Ti-6Al-4V Gyroid TPMS lattice were fabricated using selective laser melting (SLM). These lattices exhibited a high interconnected porosity ranging from 80% to 95%, with pore diameters ranging from 560 μm to 1600 μm for the Gyroid lattice. The investigation focused on the manufacturability, microstructure, and mechanical characteristics of the Ti6Al-4V TPMS lattices[(11)].

Continued on next page

Table 1 continued

5.	Fatigue behavior of As-built selective laser melted titanium scaffolds with sheet-based gyroid microarchitecture for bone tissue engineering	Kelly et al.	Evidence of a non-linear correlation between the shear strength of osseointegration and the porosity of titanium alloy gyroid implants in an ovine cortical model. The conclusion is that the porosity of the implant, and its surface area, play crucial roles in achieving stabilisation for corrosion [12].

The lowest wear rate was observed, when the sliding velocity was 4 m/s. The principal wear processes in the aforementioned three phases are delamination wear mechanism, abrasion wear mechanism and oxidation wear mechanism at low, medium, and high sliding speeds, respectively. The primary types of wear in Ti-6Al-4V alloy at 25-200 ° C includes abrasion, delamination, and adhesion wear [13]. Depending on the manufacturing methods utilized, the microstructure of a metallic material can vary greatly, which can result in a wide range of mechanical and its material characteristics as well as varying wear resistance [14]. Since the literatures available in the study of Tribology and corrosion of Additively printed Gyroid Ti-6Al-4V for implant application is scanty. This current research study was carried out to evaluate the corrosion behaviour and wear characteristics of the Gyroid lattice structure with varied porosity respectively.

Additive manufacturing has emerged as a very promising technique in the field of biomedical implants, owing to its capacity to fabricate complex structures while minimising material waste and maximising production efficiency. It facilitates the development of implants designed specifically for each patient, allowing the implant's shape to be customised to meet each person's demands. It also Enables the incorporation of porous structures into the implant, a critical aspect for achieving biological integration of the implant.

The Literature available pertaining to the corrosion and Tribological studies of Additively Printed Gyroid Ti-6Al-4V with varying porosity subjected to its different corrosion evaluation techniques viz Potentiodynamic Polarization, and the pin on disc test for the samples were evaluated respectively.

2 Materials and Methods

2.1 Direct Metal Laser Sintering (DMLS)

The chemical composition of the powder complies with the EOS Ti Grade 23 alloy, according to ASTM F3001. The Ti-Al-4V powder was supplied by EOS, Germany. which had a particle size of about 40. Ti-6Al-4V samples were created utilizing a laser powder bed fusion process using EOS M280 machine at Central Tool room and Training Centre (CTTC), Bhubaneswar, in line with ASTM B348 standard. Figure 1 depicts the pictorial representation of DMLs, a component of the Powder Bed Fusion Technique.

A Ti6Al-4V powder bed was the target of a 340W high-power laser beam, which solidified the powder after being heated locally. As a result, by incorporating material into each layer, actual 3D geometries were built in accordance with the Additive Manufacturing shaping concept and in line with ASTM 59200 - 2021.

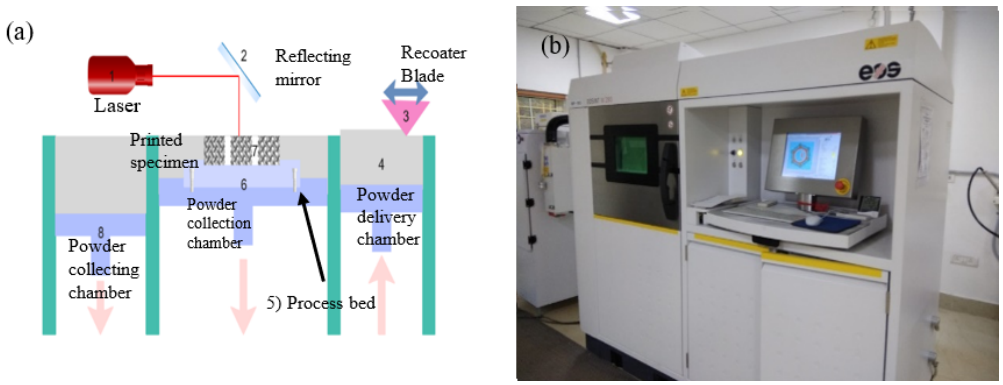

Fig 1. Direct Metal Laser Sintering

According the Luo Q et.al[15] and the machine's OEM, this inquiry picked and employed optimized process factors such as hatch distance, Laser source power, scanning speed, layer thickness has been selected.

2.2 Micro Vickers Hardness

Additively manufactured Ti-6Al-4V gyroid structured sample's hardness has been assessed using a Vickers hardness testing device (Shimatzu S200). To guarantee the uniformity of the hardness evaluation, 1000g of load and 10 seconds of dwell time, respectively, were chosen as the load and dwell times. Gyroid Ti-6Al-4V with varied porosity of 40%, 50%, and 60% samples were indented, and an average microhardness values were calculated based on a total of five measurements.

2.3 Electrochemical Corrosion Test

Potentiodynamic polarization test has been utilized to characterize the electrochemical measurement. The conventional three-electrode system consists of a working electrode that is composed of Ti-6Al-4V, a silver chloride (Ag/AgCl) acts as a reference electrode, and an auxiliary electrode made of platinum (Pt). Simulated body fluid (S.B.F.) is used as a corrosive environment. The chemical constitution of the simulated body fluid is given in Table 2. After 30 minutes of immersion in simulated bodily fluid and the corrosion behavior of orthopedic implant Ti-6Al-4V was evaluated using potentiodynamic polarization (P.D.) methods.

Table 2. The simulated body fluid's (S.B.F.) composition at 7.4 pH

Constituents	NaCl (g)	$NaHCO_3$ (g)	KCl (g)	$(CH_2OH)_3.CNH_3$ (g)	$MgCl_2.6H_2O$ (g)	1.0 HCl (ml)	$CaCl_2$ (g)	Na_2SO_4 (g)
Amount in 1000 ml	8.035	0.355	0.225	6.118	0.10	39	0.292	0.072

2.4 Pin on Disc Wear Test

The wear Test for the samples with different porosities of 40, 50 and 60 % of the samples were printed in the size of 20mm height and 10 mm diameter. The samples were printed in according to the ASTM G99 standard. The wear experiment was performed by a pin-on-disc apparatus at Metro Composites, Chennai. The sliding velocity, load, and sliding distance have been selected as the input process parameters in the Lubrication condition. The lubrication used here is Simulated Body Fluid, which can be supplied by the motor through drop-by-drop movement. The samples' wear rate and the coefficient of friction with the different condition has been recorded by the computer system.

3 Results and discussion

3.1 Micro Hardness

Hardness is one of the most routinely measured mechanical features because tests are rapid and economical, and they offer information about other properties including yield strength and wear resistance. The real influence of microstructural properties such as the existence of various phase transformation, precipitate of the particles, average grain size, and alloy composition are revealed by hardness measurements. These microstructural characteristics of a certain alloy are determined by the AM processing parameters.

Ti-6Al-4V has a microstructure composed of body-centered cubic (β) and hexagonally close-packed (α) phases, while Vanadium stabilizes the β phase, Aluminium stabilizes the α phase. The microstructures from powder bed fusion (PBF) of Additive Manufacturing (AM) often have acicular laths and a fine martensitic (α') structure. At a temperature of around 1000 $^{\circ}$C, Ti-6Al-4V changes from the Body-Centered Cubic (BCC) β phase to a two-phase structure made up mostly of Hexagonally Close-Packed (HCP) α phase and small quantities of $\alpha + \beta$ phase[16].

The microstructures of AM alloys are altered by modifications in process variables and cooling speeds. However, when the impact of the Additive Manufacturing process variables on hardness is assessed using the Hardness values that have been independently reported for manufactured components[17]. Shanmugapriya et. al has reported the Vickers Hardness for as cast Ti-6Al-4V alloy is 358 HV[18]. Thick struts possess a greater number of exposure points in comparison to their thinner counterparts. Gyroid Ti-6Al-4V Sample C has a greater thickness in its strut compared to samples A and B. The laser is intended to induce the melting of the struts located along the hatch lines. The hatch line length is seen to be shorter in thin struts, while the

modulated laser operates by targeting specific exposure spots. In the case of thin struts, a reduced amount of heat is created and subsequently accumulated. Consequently, the resulting melt pool has a tendency to assume a spherical shape. The enhancement of micro-hardness in gyroid lattice structures can be attributed to the effective metallurgical bonding between neighbouring melt pools in thick struts [19].

The hardness of the printed Gyroid lattice sample (A) with 40% porosity is 460 HV, that of the sample (B) with 50% porosity is 465 HV, while the hardness of the sample (C) with 60% porosity, which is the highest amount possible, is 467 HV as shown in the Figure 2.

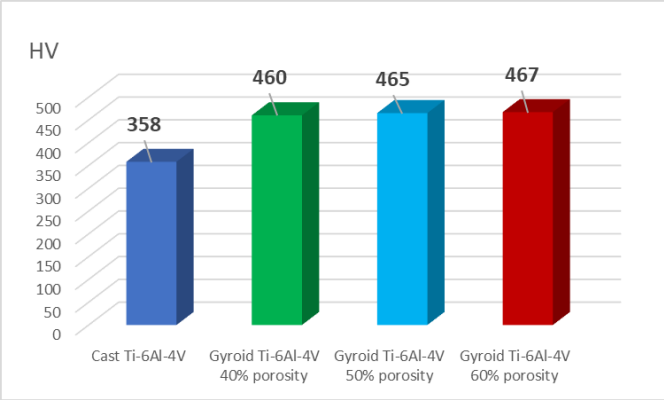

Fig 2. Microhardness of Gyroid Ti-6Al-4V

3.2 Electrochemical corrosion analysis

3.2.1 Potentiodynamic polarisation

Tafel extrapolation of the necessary polarisation parameters produced polarisation curves for Gyroid samples with different porosity, which are given in Table 3. Ti-6Al-4V had a higher Ecorr for all samples. Another important factor to take into account when selecting material for biomedical usage is the potential at which passively fractures and an anodic current greatly rises [20]. Indeed, due to the availability of chloride ions causes the passive layer to become instability at this potential, leading to localized rapid metal degradation and pitting. In this study, the Ti-6Al-4V alloy has minimal breakdown potential was discovered. Figure 3 displays the potentiodynamic polarisation curves for Gyroid heat treated Ti-6Al-4V for 2 hours at 800° C with different porosity at 7.4 pH. After allowing samples to remain submerged in the Simulated Body Fluid (SBF) for two hours at 37 °C, the potentiodynamic polarisation curves were captured.

Ali Hemmasian Ettefagh et. al [21] studied the corrosion resistance of wrought Ti-6Al-4V, as built Ti-6Al-4V and Heat treated as built Ti-6Al-4V. The Tafel extrapolation method was used to determine the samples' overall corrosion rates, which is Ecorr (V) of − 0.318 and icorr (μA/cm^2) of 0.115. The corrosion rate of this alloy is mostly influenced by the behaviour of the passive layer. The findings indicate an increase in the stability of the passive film and the decrease in the corrosion rate for the printed additive manufacturing (AM) samples when compared with wrought Ti-6Al-4V.

Ti- 6Al-4V gyroid sample (C) with 60% porosity sample after the anodic active area revealed a large stable passive zone with low current density, which suggested excellent passivity. However, when the porosity levels for sample (A) with 40% and sample (B) with 50% are in the initial passivation zone shrank and the anodic area showed evidence of a transitional interval between activation and passivation. The oxide layer that had been generated on the surfaces that were porous simultaneously became unstable. The linked passages allowed for complete liquid flow and increased corrosion-inducing contact area. Table 3 also displays the potentiodynamic polarisation parameters, which were calculated from the curves using the Tafel approximation and include current densities (Icorr), corrosion potentials (Ecorr), anodic Tafel slope (a).

3.3 Evaluation of wear behaviour on Gyroid Ti-6Al-4V

3.3.1 Impact of Load on COF and Wear Rate

Figure 4 depicts the impact of load on Friction coefficient and wear loss for Gyroid Ti-6Al-4V samples with varied porosities respectively. The maximum and minimum coefficient of friction for sample A with 40% porosity is 0.272 and 0.267. For sample B with 50% porosity is 0.33 and 0.34 and for sample C, the maximum and minimum value of friction coefficient is 0.30 and

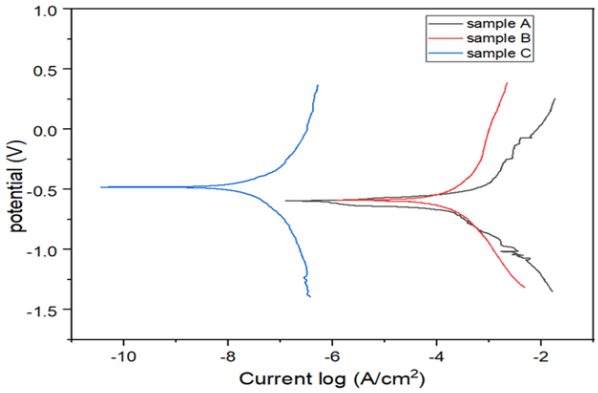

Fig 3. Potentiodynamic polarization curve for Gyroid lattice Ti-6Al-4V with different porosities in SBF at 7.4pH

Table 3. Potentiodynamic polarization parameters

Sample No	Sample Name	Icorr value (A/cm^2)	Ecorr value (obs) (V)	$\beta\alpha$ (V/dec)	βc (V/dec)	Rb (ohm)
1.	A	$1.317x10^{-3}$	-0.595	0.378	0.489	$2.439x10^{-2}$
2.	B	$1.257 x10^{-3}$	-0.589	0.588	1.248	$1.015x10^{3}$
3.	C	$3.555x10^{-7}$	-0.48	1.281	1.007	$6.304x10^{-6}$

0.38. From three samples A, B, and C, the friction coefficient increases with the load up to a load value of 30N. The material degradation on the surface of samples, A and B caused the wear rate to dramatically increase as the applied load was increased. This is because of the situation in which, under heavier loads, the melt at the interface has acted as a lubricant, significantly reducing the friction coefficient value[22]. As a result of the material hardness and improved strut thickness of the Gyroid structure in sample C, there won't be any degradation of material until 50 N.

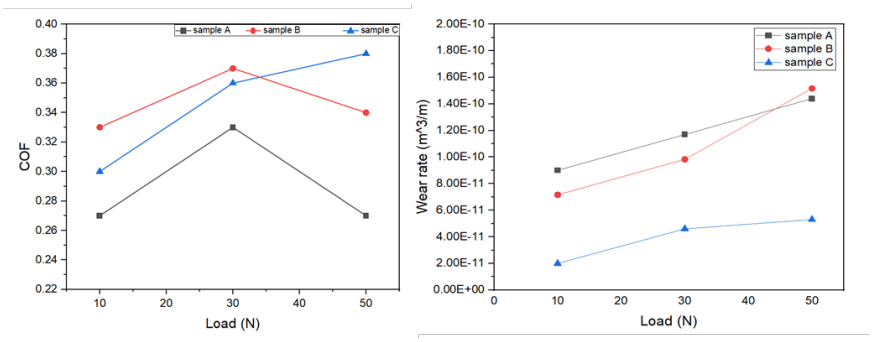

Fig 4. Impact of Load on COF and wear rate for Gyroid Ti-6Al-4V samples

Because of this condition, the coefficient of friction is elevated to 50 N. Shanmugapriya et al[23] investigated the coefficient of friction for an as-cast Titanium alloy. They found that the coefficient of friction varied from 0.2 to 0.4, indicating a high level of friction. This high friction may be attributed to the ductile behaviour of the Titanium alloy, as well as its low work hardening capability.

Table 4 displays the wear loss for Samples A, B, and C. With raise in load, the samples' wear rate rises. Sample A has a higher wear rate than Sample B. Compared to sample C, sample B shows a higher rate of wear. This is because the Gyroid structure was designed with different strut thicknesses dependent on the porosity of each sample and wear occurs with increasing load, which may be caused under hydrodynamic pressure by the contact melting[24]. The minimum wear rates for samples A, B & C are $9x10^{-11}$, $7.16x10^{-11}$, $2x10^{-11}$ m^3/m at 10N, and maximum wear rate of samples A, B & C are $1.44x10^{-11}$, $1.516x10^{-11}$, $5.3x10^{-11}$ m^3/m at 50 N respectively.

Table 4. Load vs Wear rate of Gyroid samples A, B & C

Load (N)	Wear rate (m^3 /m) for		
	sample A	Sample B	Sample C
10	9×10^{-11}	7.16×10^{-11}	2×10^{-11}
30	1.17×10^{-10}	9.83×10^{-11}	4.6×10^{-11}
50	1.44×10^{-10}	1.516×10^{-10}	5.3×10^{-11}

3.3.2 Impact of sliding velocity

The influence of velocity on friction coefficient and wear rate is seen in Figure 5. The wear rate and friction coefficient for samples A and B are rising as velocity rises. The friction coefficient in sample A is 0.28 with a velocity of 0.5 m/s, drops to 0.27 at 1 m/s, and then rapidly rises to 0.31 at 1.5 m/s.

This occurs when the sample crosses the 1 m/s velocity because a tribolayer forms on the sample's worn-out surface. Sample B has a COF of 0.33 at a velocity of 0.5 m/s; however, COF rises with respect to velocity, reaching 0.35 at 1 m/s and then 0.35 at 1.5 m/s as a result of Faster removal of wear debris occurs at higher speeds, and the detachment of wear debris may serve as a third body abrasive, considerably increasing the coefficient of friction at the point of contact [25].

The COF in sample C is 0.36 at 0.5 m/s, increases to 0.37 at 1 m/s as a result of the formation of substantial delamination and abrasion grooves on the worn-out surface, and then decreases to 0.35 of COF at 1.5 m/s.

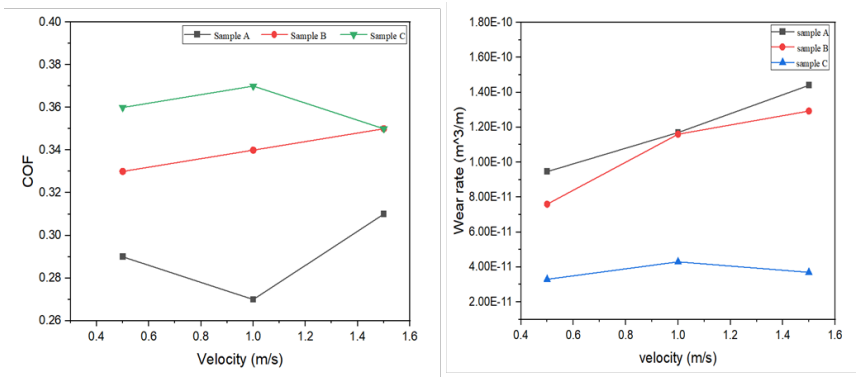

Fig 5. Impact of Velocity on COF and wear rate for Gyroid Ti-6Al-4V samples

Figure 5 depicts the wear rate of Samples A, B, and C with the influence of velocity. Samples A and B experience more wear when the velocity rises by 0.5, 1, and 1.5 m/s. The wear rate in sample C increases from 0.5 m/s to 1 m/s, then abruptly decreases beyond that point due to the

hydrodynamic lubrication of the wear debris that has built up between the sample and the revolving disc [26]. As cast Titanium alloy with the velocity of 0.5 m/s has the minimum wear rate of 4.67×10^{-7} m^3/m and the maximum wear rate of 6.45×10^{-7} m^3/m at 1.5 m/s. The printed Ti-6Al-4V Gyroid samples has less wear rate than the as cast Titanium alloy due to its finer microstructures leads to more hardness, which enhances the wear resistance respectively. Comparing samples, A and B's maximum wear rates of 1.40×10^{-10} m^3/m and 1.20×10^{-10} m^3/m at velocity of 1.5 m/s. Sample C has a maximum wear rate of 4.0×10^{-11} m^3/m at 1.5 m/s velocity. Since sample C has thicker struts than samples A and B, it is structurally more stable with regard to the point of contact. Due to this circumstance, sample C has a lower wear rate than the other two samples in the lubrication condition [27].

3.3.3 Wear Mechanism

Various wear mechanisms are explained and it is discussed on the Tribological property of Ti-6Al-4V under the lubrication condition i.e. Simulated Body Fluid (SBF).

Figure 6 **(a)** shows the Wear caused by hard fragments or surface irregularities of a hard counter body penetrating into the smoother layer of a solid object in sliding contact is known as grooving wear. Because abrasion is often the primary wear mechanism, surface damage caused by the grinding interaction of solids is frequently referred to as abrasive wear. This depicts how abrasion dominates when shear-induced fractures create debris that resembles a flake.

Figure 6**(b)** depicts the oxidation wear mechanism. The fundamental characteristic of oxidative wear is the production of an oxidative wrapping on the surface. The primary causes of oxidative film generation are changes in the working medium and temperature at the sliding contact of the material's surface. On the surface, the temperature rises by the increased sliding speeds, which leads to the creation of an oxidative coating and a quick oxidation process [28].

The wear and tear on the surface will cause the oxide layers to begin wearing after some time while sliding. The mechanism has been seen in Figure 6**(c)**. The material is moved to the worn groove's sides. The substance remains on the surface. This phenomenon is called ploughing. Even when ploughing has changed the surface, very little of the substance that has been transported ultimately splits from the surface. Deep, lengthy fissures shown on the specimen remain unchanged due to surface stress from repeated ploughing [29].

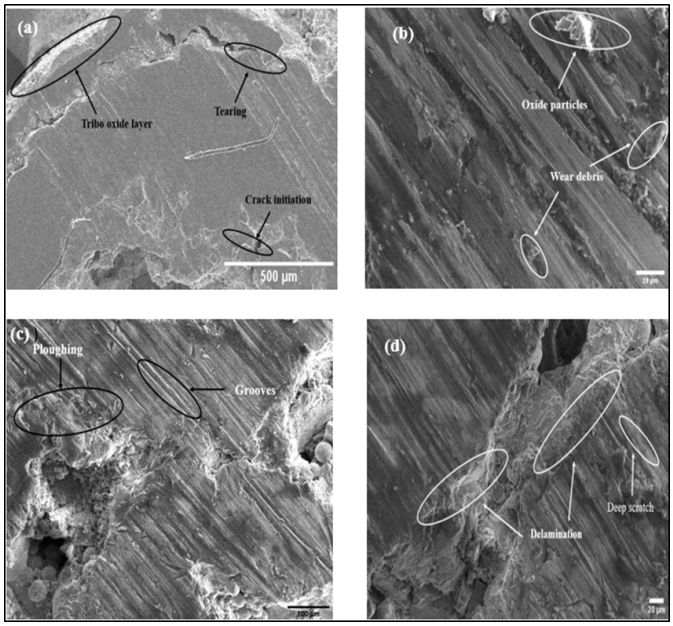

Fig 6. Wear mechanism of Gyroid Ti-6Al-4V samples- a. abrasion, b. oxidation, c. deformation, d. delamination

Figure 6**(d)** displays the delamination and deep cracks formed in the samples. It is based on the behaviour of surface-level dislocations, the creation of subsurface cracks and voids, and the subsequent merging of fractures by surface shear deformation. This surface layer can experience significant plastic deformation. The melting mechanism, which is related to chemical reactivation, emerged as a result of heat generated at the point of contact interface. Because of Ti-6Al-4V's exceptional strength, plastic deformation and fractures first appeared on worn surfaces when it was subjected to modest loads [30].

4 Conclusion

- The micro hardness for as cast Titanium alloy sample is 358 HV while the micro hardness for Gyroid Ti-6Al-4V with different porosities of samples A, B & C produced in DMLS is 460, 465 and 467 HV due to the variation in microstructures influenced by the cooling rate.
- The potyentiodynamic corrosion results proved that sample C (60% porosity) has a stable passive zone with low current density, which indicated outstanding passivity.
- The maximum corrosion rate ($1.363x10^{2}$ mm/year) and the minimum corrosion rate ($3.691x10^{-2}$ mm/year) for potentiodynamic polarisation occur at 30 minutes. The results indicate that Gyroid lattice Ti-6Al-4V with a 60% porosity exhibits the best corrosion resistance.
- The wear test results showed that sample C with 60% of porosity has more wear resistance than the sample A and B. The sample C has minimum wear rate of 2 $x10^{-11}$ m^3/m for an applied normal load of 10 N, and maximum wear rate of 5.3 $x10^{-11}$ m^3/m for normal load of 50 N. Ti-6Al-4V exhibits more wear resistance than as cast Titanium alloy.
- The future scope is further enhancing the Tribological and corrosion resistance properties. The placement of the coating needs to be performed on the Gyroid structure. The enhancement of these properties may contribute to the improvement of osseointegration and biocompatibility, hence potentially benefiting fractured applications. The implant facilitates bone

regeneration in older individuals who have experienced fractures.

References

1) Kumar R, Kumar M, Chohan JS. The role of additive manufacturing for biomedical applications: A critical review. *Journal of Manufacturing Processes*. 2021;64:828–850. Available from: https://doi.org/10.1016/j.jmapro.2021.02.022.
2) Bocchetta P, Chen LYY, Tardelli JDC, Reis ACD, Almeraya-Calderón F, Leo P. Passive Layers and Corrosion Resistance of Biomedical Ti-6Al-4V and β-Ti Alloys. *Coatings*. 2021;11(5):1–32. Available from: https://doi.org/10.3390/coatings11050487.
3) Sheoran AJ, Kumar H, Arora PK, Moona G. Bio-Medical applications of Additive Manufacturing: A Review. *Procedia Manufacturing*. 2020;51:663–670. Available from: https://doi.org/10.1016/j.promfg.2020.10.093.
4) Xiang S, Yuan Y, Zhang C, Chen J. Effects of Process Parameters on the Corrosion Resistance and Biocompatibility of Ti6Al4V Parts Fabricated by Selective Laser Melting. *ACS Omega*. 2022;7(7):5954–5961. Available from: https://doi.org/10.1021/acsomega.1c06246.
5) Sousa L, Alves AC, Costa NA, Gemini-Piperni S, Rossi AL, Ribeiro AR, et al. Preliminary tribo-electrochemical and biological responses of the Ti-TiB-TiCx in-situ composites intended for load-bearing biomedical implants. *Journal of Alloys and Compounds*. 2022;896:162965. Available from: https://doi.org/10.1016/j.jallcom.2021.162965.
6) Rezapourian M, Jasiuk I, Saarna M, Hussainova I. Selective laser melted Ti6Al4V split-P TPMS lattices for bone tissue engineering. *International Journal of Mechanical Sciences*. 2023;251:108353. Available from: https://doi.org/10.1016/j.ijmecsci.2023.108353.
7) Li H, Ramezani M, Chen ZW. Dry sliding wear performance and behaviour of powder bed fusion processed Ti–6Al–4V alloy. *Wear*. 2019;440-441:203103. Available from: https://doi.org/10.1016/j.wear.2019.203103.
8) Blanquer SBG, Werner M, Hannula M, Sharifi S, Lajoinie GPR, Eglin D, et al. Surface curvature in triply-periodic minimal surface architectures as a distinct design parameter in preparing advanced tissue engineering scaffolds. *Biofabrication*. 2017;9(2):025001. Available from: https://iopscience.iop.org/article/10.1088/1758-5090/aa6553.
9) Lu P, Wu M, Liu X, Duan W, Han J. Study on Corrosion Resistance and Bio-Tribological Behavior of Porous Structure Based on the SLM Manufactured Medical Ti6Al4V. *Metals and Materials International*. 2020;26(8):1182–1191. Available from: https://doi.org/10.1007/s12540-019-00506-w.
10) Martínez C, Briones F, Araya N, Aguilar C, Machado I, Guerra C, et al. Influence of the synthesis technique on tribological behavior of a Ti-6Al-4V alloy. *Materials Letters*. 2020;281:128627. Available from: https://doi.org/10.1016/j.matlet.2020.128627.
11) Yánez A, Herrera A, Martel O, Monopoli D, Afonso H. Compressive behaviour of gyroid lattice structures for human cancellous bone implant applications. *Materials Science and Engineering: C*. 2016;68:445–448. Available from: https://doi.org/10.1016/j.msec.2016.06.016.
12) Kelly CN, Francovich J, Julmi S, Safranski D, Guldberg RE, Maier HJ, et al. Fatigue behavior of As-built selective laser melted titanium scaffolds with sheet-based gyroid microarchitecture for bone tissue engineering. *Acta Biomaterialia*. 2019;94:610–626. Available from: https://doi.org/10.1016/j.actbio.2019.05.046.
13) Sreesha RB, Kumar D, Chandraker S, Agrawal A. Room temperature sliding wear behavior of Ti6Al4V: A review. In: MATERIALS, MECHANICS & MODELING (NCMMM-2020), 29–30 August 2020 , Jamshedpur, India;vol. 2341, Issue 1. AIP Publishing. 2021. Available from: https://doi.org/10.1063/5.0049962.
14) Wang Q, Kong J, Liu X, Dong K, Song X, Yang Y, et al. The effect of a novel low-temperature vacuum heat treatment on the microstructure and properties of Ti–6Al–4V alloys manufactured by selective laser melting. *Vacuum*. 2021;193:110554. Available from: https://doi.org/10.1016/j.vacuum.2021.110554.
15) Luo Q, Yin L, Simpson TW, Beese AM. Effect of processing parameters on pore structures, grain features, and mechanical properties in Ti-6Al-4V by laser powder bed fusion. *Additive Manufacturing*. 2022;56:102915. Available from: https://doi.org/10.1016/j.addma.2022.102915.
16) Nguyen HD, Pramanik A, Basak AK, Dong Y, Prakash C, Debnath S, et al. A critical review on additive manufacturing of Ti-6Al-4V alloy: microstructure and mechanical properties. *Journal of Materials Research and Technology*. 2022;18:4641–4661. Available from: https://doi.org/10.1016/j.jmrt.2022.04.055.
17) Khorasani A, Gibson I, Awan US, Ghaderi A. The effect of SLM process parameters on density, hardness, tensile strength and surface quality of Ti-6Al-4V. *Additive Manufacturing*. 2019;25:176–186. Available from: https://doi.org/10.1016/j.addma.2018.09.002.
18) Shanmugapriya P, Srinivasan V, Karthikeyan B, Rajamurugan TV. Surface modification of nanocomposite Al2O3/Gr/HAP coating for improving wear and corrosion behaviour on Ti–6Al–4V alloy using sol–gel technique. *Multiscale and Multidisciplinary Modeling, Experiments and Design*. 2021;4:195–205. Available from: https://doi.org/10.1007/s41939-021-00089-3.
19) Mahmoud D, Al-Rubaie KS, Elbestawi MA. The influence of selective laser melting defects on the fatigue properties of Ti6Al4V porosity graded gyroids for bone implants. *International Journal of Mechanical Sciences*. 2021;193:106180. Available from: https://doi.org/10.1016/j.ijmecsci.2020.106180.
20) Mahlobo MG, Chikosha L, Olubambi PA. Study of the corrosion properties of powder rolled Ti–6Al–4V alloy applied in the biomedical implants. *Journal of Materials Research and Technology*. 2022;18:3631–3639. Available from: https://doi.org/10.1016/j.jmrt.2022.04.004.
21) Silva D, Arcos C, Montero C, Guerra C, Martínez C, Li X, et al. A Tribological and Ion Released Research of Ti-Materials for Medical Devices. *Materials*. 2022;15(1):1–16. Available from: https://doi.org/10.3390/ma15010131.
22) Aufa AN, Hassan MZ, Ismail Z. Recent advances in Ti-6Al-4V additively manufactured by selective laser melting for biomedical implants: Prospect development. *Journal of Alloys and Compounds*. 2022;896:163072. Available from: https://doi.org/10.1016/j.jallcom.2021.163072.
23) Ettefagh AH, Zeng C, Guo S, Raush J. Corrosion behavior of additively manufactured Ti-6Al-4V parts and the effect of post annealing. *Additive Manufacturing*. 2019;28:252–258. Available from: https://doi.org/10.1016/j.addma.2019.05.011.
24) Ataee A, Li Y, Wen C. A comparative study on the nanoindentation behavior, wear resistance and in vitro biocompatibility of SLM manufactured CP–Ti and EBM manufactured Ti64 gyroid scaffolds. *Acta Biomaterialia*. 2019;97:587–596. Available from: https://doi.org/10.1016/j.actbio.2019.08.008.
25) Shanmugapriya P, Srinivasan V, Karthikeyan B, Asaithambi B. Wear Study on SOL–GEL-Coated Ti-6Al-4V Alloy. *Journal of Bio- and Tribo-Corrosion*. 2020;6(4):1–12. Available from: https://doi.org/10.1007/s40735-020-00423-1.
26) Li B, Li P, Zhou R, Feng XQQ, Zhou K. Contact mechanics in tribological and contact damage-related problems: A review. *Tribology International*. 2022;171:107534. Available from: https://doi.org/10.1016/j.triboint.2022.107534.
27) Zhang C, Zou D, Mazur M, Mo JPT, Li G, Ding S. The State of the Art in Machining Additively Manufactured Titanium Alloy Ti-6Al-4V. *Materials*. 2023;16(7):1–34. Available from: https://doi.org/10.3390/ma16072583.
28) Almeida J, Horovistiz A, Davim JP. Digital representation of the wear behaviour of Ti-6Al-4V and Ti-6Al-7Nb biomaterial alloys: A fractal analysis of the worn surface. *Proceedings of the Institution of Mechanical Engineers, Part J: Journal of Engineering Tribology*. 2023;237(5):1156–1169. Available from: https://doi.org/10.1177/1350650122114621.

29) Du D, Zhang W, An J. Two Types of Wear Mechanisms Governing Transition between Mild and Severe Wear in Ti-6Al-4V Alloy during Dry Sliding at Temperatures of 20–250 °C. *Materials*. 2022;15(4):1–21. Available from: https://doi.org/10.3390/ma15041416.
30) Gain AK, Zhang L, Lim S. Tribological behavior of Ti–6Al–4V alloy: Subsurface structure, damage mechanism and mechanical properties. *Wear*. 2021;464-465:203551. Available from: https://doi.org/10.1016/j.wear.2020.203551.